A convenient formulation of Sadowsky model for elastic ribbons

Basile Audoly, Sébastien Neukirch

A convenient formulation of Sadowsky model for elastic ribbons

Sébastien Neukirch*

d'Alembert Institute for Mechanics
CNRS & Sorbonne Université
UMR 7190, Paris, France

Basile Audoly

Laboratoire de Mécanique des Solides
CNRS, Institut Polytechnique de Paris, UMR 7649, Palaiseau, France

February 26, 2022

Elastic ribbons are elastic structures whose length-to-width and width-to-thickness aspect-ratios are both large. Sadowsky proposed a one-dimensional model for ribbons featuring a nonlinear constitutive relation for bending and twisting: it brings in both rich behaviors and numerical difficulties. By discarding non-physical solutions to this constitutive relation, we show that it can be inverted; this simplifies the system of differential equations governing the equilibrium of ribbons. Based on the inverted form, we propose a natural regularization of the constitutive law that eases the treatment of singularities often encountered in ribbons. We illustrate the approach with the classical problem of the equilibrium of a Möbius ribbon, and compare our findings to the predictions of the Wunderlich model. Overall, our approach provides a simple method for simulating the statics and the dynamics of elastic ribbons.

Keywords: boundary value problems; elastic plates; twisted rods

1. Introduction

Analyzing the equilibrium of elastic ribbons is somewhat simpler than that of elastic plates, but ribbons inherit from some of the difficulties present in elastic plates theory. One of these difficulties is the stress concentration caused by the near-inextensibility of the plate mid-surface, as found for instance in the Möbius configuration of an elastic ribbon.

In 1858, A. F. Möbius introduced its celebrated one-sided surface: a ribbon twisted and closed in such a way that its edge is a single curve. Although the Möbius strip was originally introduced as a topological curiosity, it has given rise to a challenge in elasticity theory: what is the equilibrium shape of a Möbius band made out of an elastic material? The energy functional governing the equilibrium of such an elastic ribbon, in the narrow limit, has been introduced by Sadowsky [1929], but it is only relatively recently that tractable equations for the minimization of the energy have been derived, and solved numerically, by Starostin and van der Heijden [2007]. This work initiated a surge of interest from the applied mathematics community, see for example the book edited by Fosdick and Fried [2015].

Two main difficulties arise when solving the equilibrium equations for ribbons numerically: (*i*) they are differential-algebraic equations (DAE) and (*ii*) singularities are often present in its solution. In general DAE systems are more difficult to solve than ordinary differential equations (ODE) and numerical integrators are less commonly found, and typically less optimized. Singularities in the solutions are encountered in the Möbius problem as well as in other geometries: they typically require the integration interval to be arranged (and sometimes broken down) manually in such a way the singularities lies at their endpoints, as done in past analyses of the Möbius problem [Moore and Healey, 2018; Starostin and van der Heijden, 2015].

*. Corresponding author

In this paper, we address both these problems and propose a variant of the Sadowsky model for thin elastic ribbons which takes the form of an ODE and is regularized by a small parameter.

2. EQUILIBRIUM OF ELASTIC RIBBONS (SADOWSKY MODEL)

We consider an elastic structure having length L, width w, and thickness h with $L \gg w \gg h$, see Figure 1. It is made of a linearly elastic, isotropic material with Young's module E and Poisson's ratio ν. Its deformations are computed with a one-dimensional model based on the plate bending rigidity $D = E h^3/(12(1-\nu^2))$. We work in the *special* set of units where $D\,w = 1$ and $L = 1$. The extension to a *generic* set of units involves restoring the appropriate factors $D\,w$ and L in our formulas, as found by a standard scaling analysis.

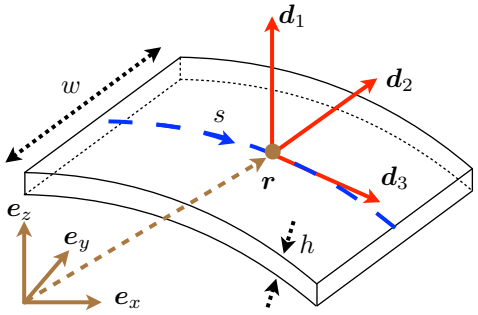

Figure 1. A ribbon with width w, thickness h is seen as a one-dimensional elastic structure with centerline $\boldsymbol{r}(s)$ and Cosserat local frame $\{\boldsymbol{d}_1(s), \boldsymbol{d}_2(s), \boldsymbol{d_3}(s)\}$, parametrized with the arclength s.

The Sadowsky model for thin, inextensible ribbons is a one-dimensional theory that is formulated as follows [Sadowsky, 1929; Starostin and van der Heijden, 2007; Dias and Audoly, 2015]. We denote as s the arc-length in reference configuration; it is used as a Lagrangian coordinate that follows material cross-sections. In actual configuration, the main unknowns are the centerline $\boldsymbol{r}(s)$ of the structure and a set of three orthonormal vectors $\{\boldsymbol{d}_1(s), \boldsymbol{d}_2(s), \boldsymbol{d_3}(s)\}$ that capture how the cross-section twists about the center-line. The combination of a center-line and a set of directors defines a so-called Cosserat rod model. Effectively, the one-dimensional model is such that the center-line is inextensible and unshearable, implying the following kinematic constraint

$$\boldsymbol{r}'(s) = \boldsymbol{d}_3(s). \tag{1}$$

The evolution of the Cosserat orthonormal frame as s is varied is given by the Darboux equation

$$\boldsymbol{d}_i'(s) = \boldsymbol{u}(s) \times \boldsymbol{d}_i(s) \qquad \text{with } 1 \leqslant i \leqslant 3 \tag{2}$$

with $\boldsymbol{u}(s)$ as the Darboux vector and $f'(s) = \frac{\mathrm{d}f}{\mathrm{d}s}$ as the derivative of a generic function $f(s)$ along the centerline. Here, the existence and unicity of $\boldsymbol{u}(s)$ follows from the orthonormal character of the frame of directors $\boldsymbol{d}_i(s)$ for any s. We work with the components $\{u_1(s), u_2(s), u_3(s)\}$ of the Darboux vector in the directors frame,

$$u_i(s) = \boldsymbol{u}(s) \cdot \boldsymbol{d}_i(s).$$

These $u_i(s)$ are the strain measures of the rod model, for bending ($i = 1, 2$) and twisting ($i = 3$).

Let us now turn to the analysis of stress in the ribbon. We denote as $\boldsymbol{n}(s)$ the force arising from the internal stress transmitted across an imaginary cut made along the cross-section with coordinate s, and $\boldsymbol{m}(s)$ the resultant moment: $\boldsymbol{n}(s)$ and $\boldsymbol{m}(s)$ are the internal force and moment, respectively. We limit attention to ribbons made of a uniform elastic material, with uniform cross-section geometry in the longitudinal direction. The constitutive relations connecting the bending and twisting strains $u_i(s)$ with the components $m_i(s) = \boldsymbol{m}(s) \cdot \boldsymbol{d}_i(s)$ of the internal moment in the directors basis write

$$u_1(s) = 0 \tag{3}$$

$$m_2(s) = u_2\left(1 - \frac{u_3^4}{u_2^4}\right) \tag{4}$$

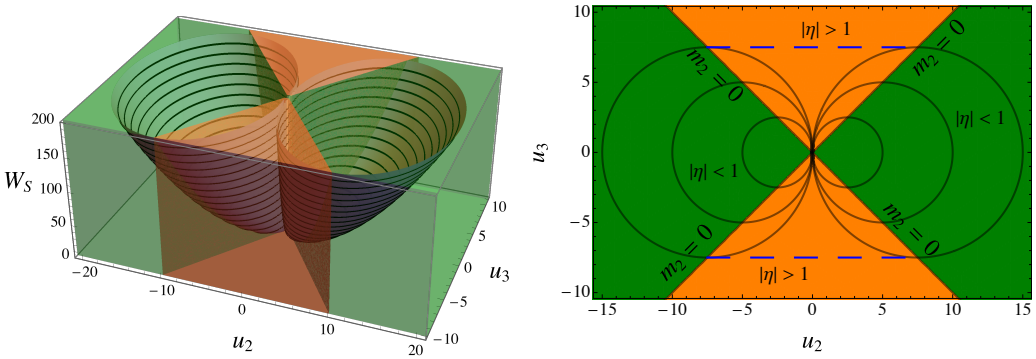

Figure 2. Sadowsky's energy surface $W_S(u_2, u_3)$ from equation (8). The energy surface is made up of two symmetric wells. Level sets are shown in black, and the 'forbidden' region corresponding to $|\eta| = |u_3/u_2| > 1$ is shaded in orange (see section 4). *Left*: three-dimensional plot. *Right*: contour plot, with a level set of the convexified functional from Freddi et al. [2015] shown in dashed blue.

$$m_3(s) \;=\; 2\,u_3\left(1+\frac{u_3^2}{u_2^2}\right). \tag{5}$$

Note that these constitutive relations are non-linear, and that the stress m_1 is absent from the first one: equation (3) is a constitutive *constraint* expressing the fact that the elastic modulus associated with bending the ribbon in its own plane is much larger than for the other bending mode.

The set of equations governing the equilibrium of the ribbon is complemented with the Kirchhoff equations for the balance of force and moment,

$$\boldsymbol{n}'(s) \;=\; \boldsymbol{0} \tag{6}$$

$$\boldsymbol{m}'(s)+\boldsymbol{r}'(s)\times\boldsymbol{n}(s) \;=\; \boldsymbol{0}. \tag{7}$$

We do not consider any distributed force or moment, such as gravity or contact forces.

The equilibrium of the ribbon can be found by solving equations (1–7) with the appropriate conditions on the boundaries $s=0$ and $s=1$.

The equilibrium problem (1–7) can be derived variationally from the constitutive constraint $u_1(s)=0$ in (3) and from the strain energy functional

$$W_S(u_2,u_3)=\frac{1}{2}\left(u_2^2+2\,u_3^2+\frac{u_3^4}{u_2^2}\right), \tag{8}$$

which is such that the constitutive relations (4-5) can be rewritten as $m_i(s)=\frac{\partial W_S}{\partial u_i}(u_2(s),u_3(s))$ for $i=2,3$. This variational derivation first appeared in [Starostin and van der Heijden, 2007]; a presentation fully in line with the theory of non-linear elastic rods has later been proposed in [Dias and Audoly, 2015].

The classical Kirchhoff rod model is recovered by changing the constitutive relations (3–5) to $m_i(s)=B_i\,u_i(s)$, for $1\leqslant i\leqslant 3$. Contrary to the case of ribbons, these constitutive relations are linear. The elastic constants B_i are the bending ($1\leqslant i\leqslant 2$) and twisting rigidities ($i=3$) of the rod. A rod with Young's modulus E, shear modulus $G=E/(2(1+\nu))$, and a rectangular cross-section (width w, thickness h) has $B_1=E\,h\,w^3/12$, $B_2=E\,h^3\,w/12$, and $B_3=G\,h^3\,w/3$, in the limit $w\gg h$.

3. Equilibrium as a differential-algebraic system

The equations for the statics of ribbons derived in section 2 form a non-linear boundary-value problem with the arclength s as independent variable, *i.e.*, a set of differential equations with boundary conditions at both endpoints $s=0$ and $s=1$.

Specifically, equations (1–7) can be written as a differential system for 6 unknowns vectors $\boldsymbol{\theta}_1$ = ($\boldsymbol{r}$, $\boldsymbol{d_1}$, $\boldsymbol{d_2}$, $\boldsymbol{d}_3$, $\boldsymbol{n}$, $\boldsymbol{m}$) plus two unknown scalars $\boldsymbol{\theta}_2$=(u_2, u_3) as

$$\begin{pmatrix}\boldsymbol{r}\\ \boldsymbol{d}_i\\ \boldsymbol{n}\\ \boldsymbol{m}\end{pmatrix}' = \begin{pmatrix}\boldsymbol{d}_3\\ (u_2\,\boldsymbol{d}_2+u_3\,\boldsymbol{d}_3)\times\boldsymbol{d}_i\\ \boldsymbol{0}\\ \boldsymbol{n}\times\boldsymbol{d}_3\end{pmatrix} \qquad\Longleftrightarrow\qquad \boldsymbol{\theta}_1'=\boldsymbol{f}(\boldsymbol{\theta}_1,\boldsymbol{\theta}_2) \tag{9a}$$

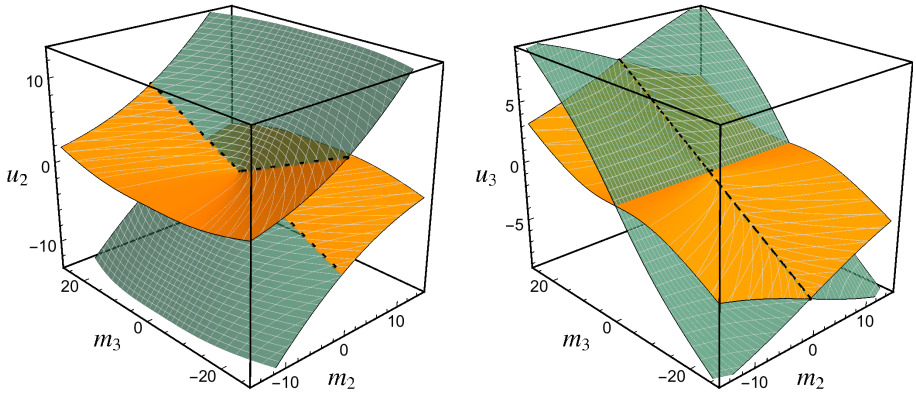

Figure 3. Inverting Sadowsky's constitutive relations. The surfaces are generated as parametric plots using the bending and twisting strain (u_2, u_3) as parameters. The bending and twisting moments (m_2, m_3) on the horizontal axes are calculated from the constitutive relation (4–5). The bending and twisting strains (u_2, u_3) are used on either one of the vertical axes. The surface is colored in green if $|\eta| < 1$ and in orange if $|\eta| > 1$, with $\eta = u_3/u_2$. The presence of two sheets stacked vertically shows that it is impossible to invert the constitutive law as $u_2 = g_2^{-1}(m_2, m_3)$ and $u_3 = g_3^{-1}(m_2, m_3)$ in general. However, this inversion becomes possible if the condition $|\eta| < 1$ is enforced, as shown by the layout of the green sections of the sheets.

$$\mathbf{0} \;=\; \begin{pmatrix} \dfrac{\partial W_S}{\partial u_2}(u_2,u_3) - \boldsymbol{m}\cdot\boldsymbol{d}_2 \\ \dfrac{\partial W_S}{\partial u_3}(u_2,u_3) - \boldsymbol{m}\cdot\boldsymbol{d}_3 \end{pmatrix} \qquad \Longleftrightarrow \qquad \mathbf{0} = \boldsymbol{g}(\boldsymbol{\theta}_1, \boldsymbol{\theta}_2). \tag{9b}$$

Due to the presence of the constraint $\boldsymbol{g}(\boldsymbol{\theta}_1, \boldsymbol{\theta}_2) = \mathbf{0}$, this problem is known as a differential-*algebraic* problem (DAE); the component form of this DAE is spelled out in Appendix A.

A difficulty is that the constitutive relation $\boldsymbol{g}(\boldsymbol{\theta}_1, \boldsymbol{\theta}_2) = \mathbf{0}$ is non-linear and *cannot* be inverted as $\boldsymbol{\theta}_2 = \boldsymbol{g}^{-1}(\boldsymbol{\theta}_1) \Leftrightarrow u_2 = g_2^{-1}(m_2, m_3)$ and $u_3 = g_3^{-1}(m_2, m_3)$. This prevents from rewriting (9) as an ordinary differential equation $\boldsymbol{\theta}_1' = \boldsymbol{f}(\boldsymbol{\theta}_1, \boldsymbol{g}^{-1}(\boldsymbol{\theta}_1))$. By contrast, for classical elastic rods (Kirchhoff rod model), the *linear* constitutive relation $\boldsymbol{g}(\boldsymbol{\theta}_1, \boldsymbol{\theta}_2) = \mathbf{0}$ *can be* inverted as $u_2 = g_2^{-1}(m_2, m_3) := m_2/B_2$ and $u_3 = g_3^{-1}(m_2, m_3) := m_3/B_3$, implying that equilibrium can be rewritten as an ordinary differential equation with $3 \times 6 = 18$ unknowns.

For thin ribbons, the impossibility to invert the constitutive relation as $u_2 = g_2^{-1}(m_2, m_3)$ and $u_3 = g_3^{-1}(m_2, m_3)$ is demonstrated graphically in figure 3. This is confirmed by the calculation from appendix B, where an attempt to invert the constitutive relations leads to multi-valued 'functions' $g_2^{-1}(m_2, m_3)$ and $g_3^{-1}(m_2, m_3)$, and therefore fails.

Numerically, the standard method for dealing with the DAE system (9) is to augment the differential equation $\boldsymbol{\theta}_1' = \boldsymbol{f}(\boldsymbol{\theta}_1, \boldsymbol{\theta}_2)$ with the differentiated form of the constraint $\boldsymbol{g} = \mathbf{0}$, namely $\frac{\partial \boldsymbol{g}}{\partial \boldsymbol{\theta}_2} \cdot \boldsymbol{\theta}_2' = -\frac{\partial \boldsymbol{g}}{\partial \boldsymbol{\theta}_1} \cdot \boldsymbol{\theta}_1'$, resulting in a ordinary differential equation with $3 \times 6 + 2 = 20$ unknowns. This is the approach chosen by several authors, see for example [Audoly and Seffen, 2015; Moulton et al., 2018; Kumar et al., 2021]. The drawback is that the resulting equations are complex; in the present work we explore a simpler approach based on the remark that the constitutive law becomes invertible when non-physical values of the strain are dismissed.

4. Inverting the constitutive law

The Sadowsky energy W_S in (8) is non-convex. As noted by Freddi et al. [2015], equations (1–7) are therefore not sufficient to warrant equilibrium. It must be required in addition that the solution lives in the region of the strain space where the solution is convex. The latter can be worked out as [Freddi et al., 2015]

$$|\eta(s)| \leqslant 1 \quad \text{where } \eta(s) = \frac{u_3(s)}{u_2(s)}. \tag{10}$$

In figures, we use the color code: green for $|\eta(s)| \leqslant 1$ and orange for the 'forbidden' region $|\eta|>1$.

A microscopic interpretation of the condition (10) can be found in [Paroni and Tomassetti, 2019], and a related discussion in the context of extensible ribbons is given in section 7 of [Audoly and Neukirch, 2021]. Note that the condition (10) amounts to replacing the Sadowsky energy W_S in equation (8) with the convexified energy W_F that matches W_S for $|\eta| \leq 1$ and is equal to $W_F(u_2, u_3) = 2\,u_3^2$ for $|\eta| \geqslant 1$ [Freddi et al., 2015]; as show in figure 2, the level sets of W_F coincide with those of W_S in the allowed region $|\eta| \leqslant 1$ but differ in the 'forbidden' region $|\eta| > 1$ (dashed blue segments in figure 2). We note that having $|\eta| > 1$ would mean obtaining a negative curvature u_2 with a positive applied bending moment m_2.

As shown by figure 3, it is possible to invert the constitutive law if one limits attention to the green portions of the surfaces, where the condition $|\eta| \leqslant 1$ holds. Closed-form expressions for the inverse constitutive law $u_2 = u_2^\star(m_2, m_3)$ and $u_3 = u_3^\star(m_2, m_3)$ are obtained as follows. We start by introducing $\lambda = \eta^2 = (u_3/u_2)^2$ and $a = m_2/m_3$. Expressing a using equations (4) by (5), we obtain $2\,a\,\eta = 1-\lambda$. Squaring both sides of this equation yields $\lambda^2 - 2\,\lambda\,(2\,a^2+1) + 1 = 0$. This equation has two real and positive roots $\lambda^\star$ and $\lambda^{\star\star}$, which are such that $0 < \lambda^\star \leqslant 1 \leqslant \lambda^{\star\star}$. The condition $|\eta| \leqslant 1$ implies $\lambda = \eta^2 \leqslant 1$ and shows that the correct root is $\lambda^\star$. This yields, after some algebra

$$\lambda^\star(m_2, m_3) = 1 + 2\,a^2 - 2\,\sqrt{a^4 + a^2} \quad \text{with } a = \frac{m_2}{m_3} \tag{11}$$

$$u_2^\star(m_2, m_3) = \frac{m_2}{(1-\lambda^\star)\,(1+\lambda^\star)} \tag{12}$$

$$u_3^\star(m_2, m_3) = \frac{m_3}{2\,(1+\lambda^\star)}. \tag{13}$$

Note the existence of a discontinuity in $u_2^\star(m_2, m_3)$ at $m_2 = 0$ when $m_3 \neq 0$, which corresponds to crossing the forbidden region shown in orange in the figures. The inverse constitutive law (12–13) yields the green surface shown in figure 4, which coincides with the green portions appearing in figure 3. It covers the first and third alternatives in Equation [6.8] of [Borum, 2018].

Using the inverse constitutive law (11–13), it is now possible to eliminate u_2 and u_3 from the differential system (9), which then takes the form of an ordinary differential equation (ODE),

$$\begin{pmatrix} \boldsymbol{r} \\ \boldsymbol{d}_i \\ \boldsymbol{n} \\ \boldsymbol{m} \end{pmatrix}' = \begin{pmatrix} \boldsymbol{d}_3 \\ (u_2^\star\,\boldsymbol{d}_2 + u_3^\star\,\boldsymbol{d}_3) \times \boldsymbol{d}_i \\ \boldsymbol{0} \\ \boldsymbol{n} \times \boldsymbol{d}_3 \end{pmatrix} \qquad \Longleftrightarrow \qquad \boldsymbol{\theta}_1' = \boldsymbol{f}^\star(\boldsymbol{\theta}_1) \tag{14}$$

The order of the differential equation is 18.

By formally setting $\lambda^\star = 0$ in equations (12–13), one recovers the inverse constitutive laws $u_2^\star = m_2$ and $u_3^\star = m_3/2$ applicable to a classical Kirchhoff rod having $B_3/B_2 = 2$. By introducing a homotopy coefficient ρ ($0 \leqslant \rho \leqslant 1$) and by replacing $\lambda^\star$ with $\rho\,\lambda^\star$ in equation (12–13), it is therefore possible to continuously change the constitutive law, from a Kirchhoff rod model with $B_1 = \infty$, $B_2 = 1$, and $B_3 = 2$ to Sadowsky's ribbon model, as shown in Appendix C. This makes it possible to treat both the Sadowsky and Kirchhoff models using the same computer code.

5. Illustration: Möbius strip

We illustrate this approach by solving the equilibrium of a Möbius strip, *i.e.*, a ribbon that is twisted by half a turn and closed into a loop. The differential equation $\boldsymbol{\theta}_1' = \boldsymbol{f}^\star(\boldsymbol{\theta}_1)$ in (14) is solved on the interval $0 \leqslant s \leqslant 1/2$, together with 18 scalar boundary conditions

$$\begin{array}{ccc} \boldsymbol{r}(0) = \boldsymbol{0} & \boldsymbol{n}(0)\cdot\boldsymbol{d}_1(0) = 0 & \boldsymbol{m}(0)\cdot\boldsymbol{d}_1(0) = 0 \\ \boldsymbol{d}_1(0) = \boldsymbol{e}_x & \boldsymbol{d}_2(0) = \boldsymbol{e}_y & \boldsymbol{d}_3(0) = \boldsymbol{e}_z \\ \boldsymbol{r}\left(\frac{1}{2}\right)\cdot\boldsymbol{e}_i = 0 \quad (i = x, y) & \boldsymbol{d}_1\left(\frac{1}{2}\right)\cdot\boldsymbol{e}_x = 0 & \boldsymbol{d}_3\left(\frac{1}{2}\right)\cdot\boldsymbol{e}_x = 0. \end{array} \tag{15}$$

The boundary conditions at $s = 1/2$ reflect the flip-symmetric nature of the solution, as assumed in previous works [Domokos and Healey, 2001; Starostin and van der Heijden, 2007; Mahadevan and Keller, 1993; Moore and Healey, 2018]. A simple shooting procedure, presented in the supplementary material, yields the components of $\boldsymbol{n}(0)$ and $\boldsymbol{m}(0)$ in the Cartesian frame as $(n_x(0), n_y(0), n_z(0)) = (0, 43.5, 42.1)$ and $(m_x(0), m_y(0), m_z(0)) = (0, 2.01, -8.87)$, as well as solution on the

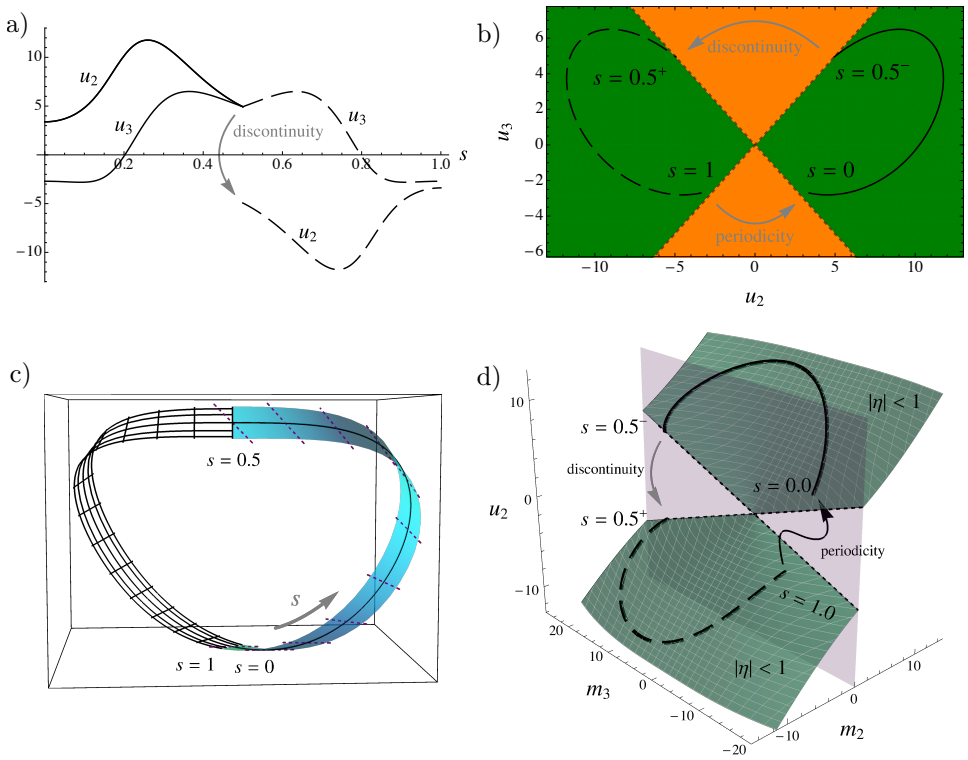

Figure 4. Möbius solution predicted by Sadowsky's model. The solution is only computed for $s \in (0; 1/2)$ (plain curves), and symmetry is used to plot the $s \in (1/2; 1)$ domain (dashed curves). (a) At the discontinuity $s = 1/2$, the curvature strain $u_2(s)$ changes sign, while the twisting strain $u_3(s)$ is continuous. (b) Parametric plot in the (u_2, u_3) plane, showing that the solution lies entirely in the region $\eta(s) \leqslant 1$ (green background). (c) Three-dimensional rendering of the Möbius solution, including the generatrices (dotted lines). (d) The parametric plot of the solution in the (m_2, m_3, u_2) space falls on the green surface predicted by the inverse constitutive law (12).

interval $0 \leqslant s \leqslant 1/2$. The solution on the other interval $1/2 \leqslant s' \leqslant 1$ is then generated by symmetry, using $u_2(s') = -u_2(1 - s')$ and $u_3(s') = +u_3(1 - s')$.

In figure 4a, the solutions $u_2(s)$ and $u_3(s)$ are plotted. The point $s = 1/2$ is a discontinuity where u_2 flips sign while u_3 remains continuous. At the discontinuity, $|u_2((1/2)^{\pm})| = |u_3(1/2)|$, implying that $\eta(s)$ jumps from $+1$ at $s = (1/2)^-$ to -1 at $s = (1/2)^+$. In the space (u_2, u_3) shown in figure 4b, the discontinuity causes a jump across the forbidden region, as shown by the gray arrow. In the space (m_2, m_3, u_2) it causes a jump from one green sheet to the other, see figure 4d. The equilibrium imposes that the components $m_2(s)$ and $m_3(s)$ of the internal moment are continuous at the discontinuity.

Let us now turn to the periodicity condition at the $s = 1$ endpoint. As the Möbius strip is not orientable, the directors $\boldsymbol{d}_1$ and $\boldsymbol{d}_2$ are opposite to each other there, $\boldsymbol{d}_i(1) = -\boldsymbol{d}_i(0)$ for $i = 1, 2$. Even though the Darboux vector $\boldsymbol{u}$ is continuous, $\boldsymbol{u}(1) = \boldsymbol{u}(0)$, the non-orientability creates an apparent jump in the bending and twisting strains $u_i(1) = -u_i(0)$ for $i = 1, 2$, materialized by the second arrow in figures 4b,d.

We have recovered the solution of the Möbius problem predicted by the Sadowsky model, that appeared in previous works, using a simple, constraint-free formulation (14). The singularity $s = 1/2$ has been placed at an *endpoint* of the mathematical domain $s \in (0, 1/2)$ on which we solved the boundary-value problem (15). In this happy but somewhat peculiar situation, there is no discontinuity inside the simulation domain $(0, 1/2)$. In general, however, the solutions of Sadowsky's model may feature interior discontinuities, and they must be taken care of by means of special jump conditions, see [Freddi et al., 2015] as well as section 7 in [Audoly and Neukirch, 2021]. Interior discontinuities may appear under various loading conditions, and have been reported by [Yu and Hanna, 2019; Huang et al., 2020; Charrondière et al., 2020]. As the position of an interior discontinuity is not known *a priori* in the absence of symmetry, dealing with them requires additional work.

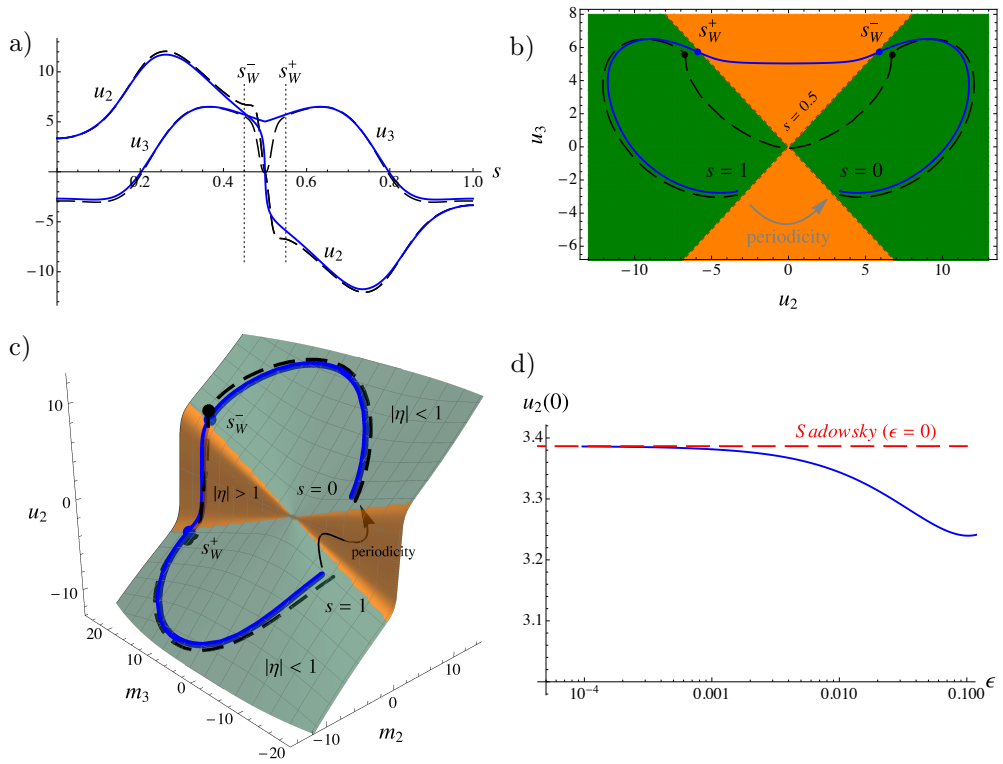

Figure 5. Solution of the regularized Sadowsky model from section 6 for $\varepsilon = 0.01$ (solid blue curves) for a Möbius band, and comparison to the Wunderlich model (dashed black curves). The points $W^{\pm}$ are where the solution of the regularized Sadowsky model enters or exits the forbidden zone $|\eta| > 1$. (a) Bending and twisting strain, $u_i(s)$. (b) Parametric plot in the (u_2, u_3) plane. (c) Parametric plot in the (m_2, m_3, u_2) space, and comparison with the regularized constitutive law (16) (surface) (d) Convergence of the value $u_2(0)$ predicted by the regularized Sadowsky model (blue curve) to that predicted by the original Sadowsky model (red). The data for the Wunderlich solution is taken from [Starostin and van der Heijden, 2015], see the green curve of their Figure 7, with $w/L = 0.2/\pi$.

6. Smoothing discontinuities

In this section, we present a method that avoids dealing with interior discontinuities. We observe that the inverse constitutive law $u_2 = u_2^\star(m_2, m_3)$ in equation (12) can be regularized as follows

$$u_2^\star(m_2, m_3, \varepsilon) = \frac{m_2}{(1 - \lambda^\star + \varepsilon)\,(1 + \lambda^\star)}. \tag{16}$$

We have introduced a small regularizing parameter $\varepsilon > 0$ in the denominator, such that the Sadowsky model is recovered in the limit $\varepsilon \to 0$. This regularization corresponds to going from the discontinuous surface shown in figure 4c, to the smooth one shown in figure 5c for $\varepsilon = 0.01$. Note that this regularized constitutive law suppresses interior discontinuities, but puts an end to the variational nature of the model.

For the Möbius problem, it is now possible to solve the differential system (14) on the *entire* interval $s \in (0, 1)$. Using the smoothed constitutive law (16) for u_2 and the original constitutive law (13) for u_3, together with the clamped boundary conditions

$$\begin{array}{llll} \boldsymbol{r}(0) = \boldsymbol{0} & \boldsymbol{d}_1(0) = \boldsymbol{e}_x & \boldsymbol{d}_2(0) = \boldsymbol{e}_y & \boldsymbol{d}_3(0) = \boldsymbol{e}_z \\ \boldsymbol{r}(1) = \boldsymbol{0} & \boldsymbol{d}_1(1) \cdot \boldsymbol{d}_2(0) = 0 & \boldsymbol{d}_2(1) \cdot \boldsymbol{d}_3(0) = 0 & \boldsymbol{d}_3(1) \cdot \boldsymbol{d}_1(0) = 0, \end{array} \tag{17}$$

we did obtain the solution of the regularized problem over the entire interval $s \in (0, 1)$ directly, by a shooting method. The initial values for $\varepsilon = 0.01$ were obtained numerically as $(n_x(0), n_y(0), n_z(0)) = (0, 43.1, 43.0)$ and $(m_x(0), m_y(0), m_z(0)) = (0, 2.15, -8.65)$. This solution is shown by the solid blue curves in figure 5. Details on the numerical solution are provided in the supplementary material.

Note that the equilibrium equations (7), together with the periodic conditions for $\boldsymbol{r}(s)$ in (17) suffice to warrant that both $\boldsymbol{n}(s)$ and $\boldsymbol{m}(s)$ are periodic. Replacing the condition $x(1)=0$ with $n_1(0)=0$ helps the numerical resolution of the BVP by removing its s invariance.

The convergence of the solution of the regularized problem towards the solution of the original Sadowsky problem for $\varepsilon \to 0$ is checked in figure 5d, where the value of $u_2(0)$ is plotted as a function of ε. The limiting value $u^0_{2,S} = 3.3866$ predicted by the original Sadowsky model is recovered asymptotically for $\varepsilon \to 0$.

From figure 5c, it appears that the solution still switches from the upper green layer to the lower green layer across the mid-point $s=1/2$ but this transition now takes place smoothly. As shown in figure 5b, the regularized solution does enter the region $|\eta|>1$ that was forbidden in the original Sadowsky model, near the smoothed discontinuity $s=1/2$.

In figure 5, this solution is also compared to the solution of the more accurate—but also numerically more challenging—Wunderlich model, governed by the functional

$$W_W(u_2,u_3) = W_S(u_2,u_3)\,\frac{1}{\eta' w}\log\left(\frac{2+\eta' w}{2-\eta' w}\right) \tag{18}$$

where $\eta(s) = u_3(s)/u_2(s)$ and with $w/L = 0.2/\pi$, see [Wunderlich, 1962]. The Wunderlich energy W_W includes a gradient term $\eta'(s)$ that regularizes the discontinuities found in Sadowsky's model: the Wunderlich solutions feature an inner layer near $s=1/2$. The detailed features of the inner layer of the Wunderlich solution are different from those of the regularized Sadowsky model, as shown by a comparison of the dashed black and solid blue curves near $s=1/2$ (see in particular figure 5b). This could be expected from the fact that the Wunderlich model is designed to resolve the boundary layer accurately, the original Sadowsky model ignores it, and the regularized Sadowsky model provides a convenient but non-principled regularization. Still, the main point is that away from the smoothed discontinuity at $s=1/2$, the solutions to the Sadowsky and Wunderlich models are similar [Starostin and van der Heijden, 2015; Kumar et al., 2021]: this can be seen here by comparing Figures 4 and 5.

7. Conserved quantities

We return to the original (non-regularized) Sadowsky model. Invariants have been extensively studied in Kirchhoff rods. In both Kirchhoff rods and ribbons that are free of any external load, the quantities $\boldsymbol{n}(s)$ and $\boldsymbol{n}(s)\cdot\boldsymbol{m}(s)$ are constant: this follows directly from the equations of equilibrium (6–7). There exists yet another conserved quantity, introduced as a Hamiltonian by Kehrbaum and Maddocks [1997] and derived in [Starostin and van der Heijden, 2015] for ribbons. It is defined through a Legendre transformation W_{Leg} of the strain energy W_S:

$$\begin{aligned} W^\star(m_2,m_3,u_2,u_3) &= m_2\,u_2 + m_3\,u_3 - W_S\,(u_2,u_3) \\ W_{\text{Leg}}(m_2,m_3) &= \sup_{u_2,u_3} W^\star(m_2,m_3,u_2,u_3) \\ H(n,m) &= W_{\text{Leg}}(m_2,m_3) + n_3. \end{aligned} \tag{19}$$

The Hamiltonian H is a conserved quantity: it satisfies $\frac{\mathrm{d}H}{\mathrm{d}s}=0$ for any s, when evaluated on an equilibrium solution. In the equations above, $n_i = \boldsymbol{n}\cdot\boldsymbol{d}_i$, and $m_i = \boldsymbol{m}\cdot\boldsymbol{d}_i$ denote the components of the internal force and moment in the directors basis.

In equation (19), we consider the case where the supremum over (u_2,u_3) is attained, *i.e.*, it is a maximum of $W^\star$: this implies that $\frac{\partial W^\star}{\partial u_2}=0$ and $\frac{\partial W^\star}{\partial u_3}=0$, which yields exactly the constitutive relations (4) and (5). As discussed in Section 3, for every value of (m_2,m_3), there are two corresponding solutions (u_2,u_3) by the constitutive relations; this leads to the two sheets in the three-dimensional plots. The solution set (u_2,u_3) that actually achieve the maximum in (19) is precisely that given by (12) and (13). We can then explicitly calculate W_{Leg} and find

$$W_{\text{Leg}}(m_2,m_3) = \frac{1}{8}\left(\sqrt{m_2^2}+\sqrt{m_2^2+m_3^2}\right)^2 \tag{20}$$

In terms of u_2 and u_3, this quantity evaluates to $W_{\text{Leg}} = \frac{1}{2} u_2^2 (1 + \frac{u_3^2}{u_2^2})^2 = W_S$, as noticed in [Starostin and van der Heijden, 2015]. Equation (20) corresponds to choosing a plus sign in [C.14] of [Borum, 2018].

For the Möbius solution from section 5, for instance, we find the value of the invariant to be $H = 57.5$.

8. Conclusion

We have shown that the two main issues associated with Sadowsky's model for elastic ribbons, namely the differential-algebraic nature of the equilibrium equations and the singularity arising at inflection points ($u_2(s) = 0$) can both be overcome by using a regularized and inverted constitutive relation. We have illustrated our approach on the Möbius configuration, and have shown that the regularized model converges toward Sadowsky's model when the regularization parameter goes to zero. We note that other ways to regularize Sadowsky's equations have been used [Sano and Wada, 2019] but they only *postpone* the occurrence of the singularity which eventually arises for large enough strain. We have compared the equilibrium solution found with our model to the solution found with Wunderlich's model and we have shown that they only differ in the region where the singularity occurs: in Wunderlich's model the twist strain (u_3) is forced to vanish at the singular point (where $u_2 \to 0$) in order to leave the ratio $\eta(s) = u_3(s)/u_2(s)$ finite, while this is not the case in our approach. Besides, equilibrium equations in Wunderlich's model comprise a differential equation for the ratio $\eta(s)$ that can prove delicate to handle numerically: see for example [Moore and Healey, 2018] where a special fix has been introduced to lessen the numerical stiffness and be able to cross the singular event. By contrast, our approach has no such difficulties and crossing singular points is easy. In future work, it will be interesting to analyze equilibria featuring multiple singularities [Yu and Hanna, 2019; Huang et al., 2020] and singularities for ribbons possessing natural curvature [Charrondière et al., 2020] using our model.

Acknowledgments

It is a pleasure to thank G. van der Heijden for providing numerical data for solutions with Wunderlich's model, as well as G. van der Heijden and A. Borum for providing feedback on the manuscript.

Appendix A. Statics in components form

The differential equations (9a) governing the equilibrium can be spelled out in components as

$$\begin{aligned}
x' &= d_{3x} & n_1' &= n_2 u_3 - n_3 u_2 \\
y' &= d_{3y} & n_2' &= n_3 u_1 - n_1 u_3 \\
z' &= d_{3z} & n_3' &= n_1 u_2 - n_2 u_1 \\
d_{3x}' &= u_2 d_{1x} - u_1 d_{2x} & m_1' &= m_2 u_3 - m_3 u_2 + n_2 \\
d_{3y}' &= u_2 d_{1y} - u_1 d_{2y} & m_2' &= m_3 u_1 - m_1 u_3 - n_1 \\
d_{3z}' &= u_2 d_{1z} - u_1 d_{2z} & m_3' &= m_1 u_2 - m_2 u_1 \\
d_{1x}' &= u_3 d_{2x} - u_2 d_{3x} & d_{2x}' &= u_1 d_{3x} - u_3 d_{1x} \\
d_{1y}' &= u_3 d_{2y} - u_2 d_{3y} & d_{2y}' &= u_1 d_{3y} - u_3 d_{1y} \\
d_{1z}' &= u_3 d_{2z} - u_2 d_{3z} & d_{2z}' &= u_1 d_{3z} - u_3 d_{1z}.
\end{aligned} \tag{21}$$

As explained in section 3,

- for classical Kirchhoff rods, the inverse constitutive relations $u_i(s) = m_i(s)/B_i$ can be inserted directly, which yields an ordinary differential equation of order 18;
- for a Sadowsky ribbon, one option is to complement these equations with the 3 constitutive relation (3–5), which yields a DAE with 21 unknowns.

APPENDIX B. MULTI-VALUED INVERSION

After some algebra, the constitutive relations (4–5) can be inverted as

$$u_2(m_2,m_3) = \frac{\chi}{4}\frac{m_3^4\sqrt{m_2^2+m_3^2}}{\left(m_2^2+m_3^2+m_2\,\chi\sqrt{m_2^2+m_3^2}\right)^2} \tag{22a}$$

$$u_3(m_2,m_3) = \frac{1}{4}\frac{m_3^3}{m_2^2+m_3^2+m_2\,\chi\sqrt{m_2^2+m_3^2}} \tag{22b}$$

where $\chi = \pm 1 = \mathrm{sign}(u_2(s=0))$. See also [Borum, 2018] for alternate, equivalent expressions.

The plot in Figure 3 has been generated as parametric plot, as explained in the legend, but it is also possible to generate it using the formulas above: the existence of two sheets corresponds to the choice of $\chi = \pm 1$ in the formulas above.

APPENDIX C. HOMOTOPY FROM RODS TO RIBBONS

We use the homotopy coefficient $\rho \in (0;1)$ and replace $\lambda^\star$ with $\rho\,\lambda^\star$ in (12–13) to continuously pass from a rod model (having $B_1 = \infty$, $B_2 = 1$, and $B_3 = 2$) to a ribbon model:

$$\begin{aligned} u_2^\star(m_2,m_3,\varepsilon,\rho) &= \frac{m_2}{(1-\rho\,(\lambda^\star-\varepsilon))\,(1+\rho\,\lambda^\star)} \\ u_3^\star(m_2,m_3,\rho) &= \frac{m_3}{2\,(1+\rho\,\lambda^\star)} \end{aligned} \tag{23}$$

with $\rho = 0$ for rods, and $\rho = 1$ for ribbons.

BIBLIOGRAPHY

[Audoly and Neukirch, 2021] B. Audoly and S. Neukirch. A one-dimensional model for elastic ribbons: a little stretching makes a big difference. *Journal of the Mechanics and Physics of Solids*, 153: 104457, 2021.

[Audoly and Seffen, 2015] B. Audoly and K. A. Seffen. Buckling of naturally curved elastic strips: The ribbon model makes a difference. *Journal of Elasticity*, 119 (1): 293–320, 2015.

[Borum, 2018] A. Borum. *Manipulation and mechanics of thin elastic objects*. PhD thesis, University of Illinois at Urbana-Champaign, 2018.

[Charrondière, Bertails-Descoubes, Neukirch, and Romero, 2020] R. Charrondière, F. Bertails-Descoubes, S. Neukirch, and V. Romero. Numerical modeling of inextensible elastic ribbons with curvature-based elements. *Computer Methods in Applied Mechanics and Engineering*, 364: 112922, 2020.

[Dias and Audoly, 2015] M. A. Dias and B. Audoly. 'Wunderlich, meet Kirchhoff': A general and unified description of elastic ribbons and thin rods. *Journal of Elasticity*, 119 (1-2): 49–66, 2015.

[Domokos and Healey, 2001] G. Domokos and T. Healey. Hidden symmetry of global solutions in twisted elastic rings. *Journal of Nonlinear Science*, 11: 47–67, 2001.

[Fosdick and Fried, 2015] R. Fosdick and E. Fried, editors. *The Mechanics of Ribbons and Moebius Bands*, 2015. Springer.

[Freddi, Hornung, Mora, and Paroni, 2015] L. Freddi, P. Hornung, M.-G. Mora, and R. Paroni. A corrected Sadowsky functional for inextensible elastic ribbons. *Journal of Elasticity*, 123: 125–136, 2015.

[Hinz and Fried, 2015] D. F. Hinz and E. Fried. Translation of Michael Sadowsky's Paper "The Differential Equations of the Möbius Band". *Journal of Elasticity*, 119 (1): 19–22, 2015.

[Huang, Wang, Li, and Jawed, 2020] W. Huang, Y. Wang, X. Li, and M. K. Jawed. Shear induced supercritical pitchfork bifurcation of pre-buckled bands, from narrow strips to wide plates. *Journal of the Mechanics and Physics of Solids*, 145: 104168, 2020.

[Kehrbaum and Maddocks, 1997] S. Kehrbaum and J. H. Maddocks. Elastic rods, rigid bodies, quaternions and the last quadrature. *Philosophical Transactions of the Royal Society of London. Series A, Mathematical and Physical Sciences*, 355 (1732): 2117–2136, 1997.

[Kumar, Handral, Bhandari, and Rangarajan, 2021] A. Kumar, P. Handral, D. Bhandari, and R. Rangarajan. More views of a one-sided surface: mechanical models and stereo vision techniques for Möbius strips. *Proceedings of the Royal Society A: Mathematical, Physical and Engineering Sciences*, 477 (2250): 20210076, 2021.

[Mahadevan and Keller, 1993] L. Mahadevan and J. B. Keller. The Shape of a Möbius band. *Proc. R. Soc. Lond. A*, 440: 149–162, 1993.

[Moore and Healey, 2018] A. Moore and T. Healey. Computation of elastic equilibria of complete Möbius bands and their stability. *Mathematics and Mechanics of Solids*, 24 (4): 939–967, 2018.

[Moulton, Grandgeorge, and Neukirch, 2018] D. E. Moulton, P. Grandgeorge, and S. Neukirch. Stable elastic knots with no self-contact. *Journal of the Mechanics and Physics of Solids*, 116: 33 – 53, 2018.

[Paroni and Tomassetti, 2019] R. Paroni and G. Tomassetti. Macroscopic and microscopic behavior of narrow elastic ribbons. *Journal of Elasticity*, 135: 409–433, 2019.

[Sadowsky, 1929] M. Sadowsky. Die Differentialgleichungen des MÖBIUSschen Bandes. *Jahresbericht der Deutschen Mathematiker-Vereinigung*, 39: 49–51, 1929. Translated in [Hinz and Fried, 2015].

[Sano and Wada, 2019] T. G. Sano and H. Wada. Twist-induced snapping in a bent elastic rod and ribbon. *Phys. Rev. Lett.*, 122: 114301, 2019.

[Starostin and van der Heijden, 2007] E. L. Starostin and G. H. M. van der Heijden. The shape of a Moebius strip. *Nature Materials*, 6 (8): 563–567, 2007.

[Starostin and van der Heijden, 2015] E. L. Starostin and G. H. M. van der Heijden. Equilibrium Shapes with Stress Localisation for Inextensible Elastic Möbius and Other Strips. *Journal of Elasticity*, 119 (1): 67–112, 2015.

[Todres, 2015] R. E. Todres. Translation of W. Wunderlich's "On a Developable Möbius Band". *Journal of Elasticity*, 119 (1): 23–34, 2015.

[Wunderlich, 1962] W. Wunderlich. Über ein abwickelbares Möbiusband. *Monatshefte für Mathematik*, 66 (3): 276–289, 1962. Translated in [Todres, 2015].

[Yu and Hanna, 2019] T. Yu and J. A. Hanna. Bifurcations of buckled, clamped anisotropic rods and thin bands under lateral end translations. *Journal of the Mechanics and Physics of Solids*, 122: 657–685, 2019.